Tellus (2002), 54A, 107–123
Printed in UK. All rights reserved

TELLUS
ISSN 0280–6495

A new parameterization of surface drag in the marginal sea ice zone

By GERIT BIRNBAUM* and CHRISTOF LÜPKES, *Alfred Wegener Institute for Polar and Marine Research, Postfach 120161, D-27515 Bremerhaven, Germany*

(Manuscript received 31 August 2000; in final form 18 June 2001)

ABSTRACT

A parameterization of subgridscale surface fluxes over the marginal sea ice zone which has been used earlier in several studies is modified and applied to a nonhydrostatic mesoscale model. The new scheme accounts for the form drag of ice floes and is combined with a so-called flux averaging method for the determination of surface fluxes over inhomogeneous terrain. Individual fluxes over ice and water are calculated as a function of the blending height. It is shown by comparison with observations that the drag coefficients calculated with the new parameterization agree well with data. The original scheme strongly overestimates the form drag effect. An improvement is mainly obtained by an inclusion of stratification and by use of a more adequate coefficient of resistance for individual ice floes. The mesoscale model is applied to off-ice flows over the polar marginal sea ice zone. The model results show that under certain meteorological conditions the form drag can have a strong influence on the near-surface wind velocity and on the turbulent fluxes of momentum. Four case studies are carried out. The maximum influence of form drag occurs in the case with strong unstable stratification and with wind oblique to the ice edge. Under these conditions the wind stress on sea ice is modified by at least 100% for ice concentrations less than 50% if form drag is taken into account.

1. Introduction

In the marginal sea ice zone (MIZ), which is the transition zone between the polar pack ice and the open ocean, sea ice strongly influences the transport of momentum, heat and moisture between atmosphere and ocean. Dynamic forces exerted by wind and ocean currents on sea ice considerably depend on the morphology and especially on the size and the distribution of ice floes and pressure ridges. The increased atmospheric shear stress over the MIZ caused by the dynamic pressure of floe edges and ridges is taken into account by several concepts of different complexities.

The most simple approach prescribes an increased roughness length (e.g., Wefelmeier, 1992) in the MIZ to account for the increased roughness due to floe edges. A more sophisticated concept originally developed for closed pack ice regions with pressure ridges was first introduced by Arya (1975) and later used, e.g., by Dierking (1995) as well as Garbrecht et al. (1999). Arya partitions the total surface drag into the contributions of skin drag and form drag. The skin drag represents the surface drag of an area with obstacles considerably lower than the average height of the larger obstacles which cause the form drag. In contrast to Arya (1975), Hanssen-Bauer and Gjessing (1988) (H-BG 88 hereafter) establish a concept suitable for a broken ice cover which treats the influence of floe edges on the form drag but neglects pressure ridges. Mai et al. (1996) provide an optimized drag partitioning model accounting for the floe edge as well as for the pressure ridge

* Corresponding author.
e-mail: gbirnbaum@awi-bremerhaven.de

effect by combining the models of Arya (1975) and H-BG 88. Mai et al. (1996) found for the MIZ in the Fram Strait region that the form drag caused by floe edges amounted up to 40% of the skin drag, while the form drag caused by pressure ridges on the floes located off the floe edges never exceeded 10%. However, Garbrecht et al. (1999) show that the form drag of ridges can amount up to 50% of the skin drag over regions with ice concentrations larger than 95% and even more next to coastal barriers.

In the present paper, a revised and extended version of the concept of H-BG 88 is developed which is applicable in the MIZ. The new concept which we use in a nonhydrostatic mesoscale atmospheric model accounts for ridges at the floe edges and includes effects of thermal stratification in the determination of the form drag. Furthermore, we apply a coefficient of resistance for ice floes which is based on observations over ice ridges. Turbulent surface fluxes over the MIZ are calculated as a function of the blending height, which is defined as the height at which the flow changes from equilibrium with the local surface to independence of horizontal position. Within our new concept the blending height is influenced by form drag. Both schemes, the new one and the original one of H-BG 88, are used in the mesoscale model, and the modelled drag coefficients are compared with aircraft-observed data. The model is applied to off-ice flows over typical Arctic marginal ice zones which develop during cold-air outbreaks.

The outline of the paper is as follows. In Section 2 we summarize the main features of the used model. In Section 3 the new surface drag concept for the MIZ is presented. Model runs and results are explained in Sections 4, 5 and 6. A comparison of modelled and observed drag coefficients and a study of the model sensitivity to various assumptions of the new parameterization are presented.

2. Model description

The nonhydrostatic and anelastic atmospheric model METRAS (Schlünzen, 1988, 1990) is used in the same 2D version as applied earlier to Arctic cold-air outbreaks by Lüpkes and Schlünzen (1996). Hence, we only provide a short description of the model characteristics.

The model is based on the Boussinesq-approximated primitive equations with potential temperature, specific humidity and three wind components as prognostic variables. Within the present study, it is applied to situations with strong surface forcing. Radiation is not taken into account for simplicity. Furthermore, we neglect phase changes of humidity. However, specific humidity can reach its saturation value and even higher values.

Horizontal turbulent transport is neglected with respect to the horizontal grid size ($\Delta x = 4$ km), numerical schemes and horizontal filtering. A simple nonlocal closure scheme (Lüpkes and Schlünzen, 1996) which includes countergradient fluxes of heat and humidity is used for the parameterization of vertical turbulent fluxes in the convective boundary layer. In case of stable stratification and above the convective boundary layer a simple mixing length scheme is applied (Herbert and Kramm, 1985).

The model equations are solved on a staggered ARAKAWA-C grid. The nonuniform vertical grid size varies between 20 m and 50 m below 1500 m. Above this level, it increases by a factor of 1.15 up to a maximum value of 1000 m. The first scalar grid point above the surface is at 10 m height. The model top is at 11 000 m.

The surface temperature is prescribed constant in time, and water vapour saturation is assumed at the surface. At lateral boundaries, boundary-normal gradients of boundary-parallel wind components as well as potential temperature and specific humidity are prescribed to zero. The boundary-normal wind is derived from the prognostic momentum balance equations.

For initialization, the model requires the large scale geostrophic wind as well as quasi-stationary profiles of potential temperature and humidity at the inflow boundaries. Such profiles can be determined with the 1D model version based on observed or prescribed meteorological variables and profiles.

3. Parameterization of surface drag in the MIZ

3.1. *Parameterization of form drag*

The force exerted from the air on ice floes consists of a pressure force (normal component)

and a frictional force (tangential component). According to Arya (1975) these components are equivalent to the form drag and the skin drag. Assuming that they point into the same direction, the total drag of sea ice is given by the sum of form drag and skin drag.

Our calculation of the form drag in the MIZ is an extension of the approach of H-BG 88. In their concept, ice floes have a flat surface and a quadratic base. The air flow direction is normal to the windward floe edges which cause the form drag. In our extended concept, we additionally assume small pressure ridges at the upstream and downstream floe edges (Fig. 1). This is justified by aircraft based laser altimeter observations in the Arctic MIZ (Kottmeier et al., 1994). They show that on average the largest ridges of about 25 cm height occur at the floe edges. We further assume, consistent with findings of Mai et al. (1996), that the smaller ridges on the interior of floes contribute to the skin drag only, whereas the ridges at the floe edges contribute to the form drag. With these assumptions the form drag can be derived similar to H-BG 88 as

$$F_{\mathrm{d}} = \frac{\rho}{2}\frac{c_{\mathrm{w}}}{L_{\mathrm{i}}+L_{\mathrm{w}}}\left[1-\exp\left(-0.18\,\frac{L_{\mathrm{w}}}{H_{\mathrm{f}}}\right)\right]^2 \times \frac{u_{*\mathrm{w}}^2}{\kappa^2}\int_{z_{0\mathrm{w}}}^{H_{\mathrm{f}}}\left[\ln\left(\frac{z}{z_{0\mathrm{w}}}\right)-\psi_{\mathrm{m,w}}\right]^2 \mathrm{d}z + \frac{\rho}{2}\frac{c_{\mathrm{w}}}{L_{\mathrm{i}}+L_{\mathrm{w}}}\left[1-\exp\left(-0.18\,\frac{L_{\mathrm{i}}}{H_{\mathrm{r}}}\right)\right]^2 \times \frac{u_{*\mathrm{i}}^2}{\kappa^2}\int_{z_{0\mathrm{i}}}^{H_{\mathrm{r}}}\left[\ln\left(\frac{z}{z_{0\mathrm{i}}}\right)-\psi_{\mathrm{m,i}}\right]^2 \mathrm{d}z. \quad (1)$$

This parameterization still includes the H-BG 88 empirical correction for the reduction of wind velocity downstream of ridges, but additionally takes into account stability corrected wind profiles [e.g., Dyer (1974)]. In eq. (1), H_{f} is the grid cell averaged freeboard height at the windward floe edge (distance between the water surface and the top of the ridge) and H_{r} is the pressure ridge height at the leeward floe edge (distance between the flat inner ice floe surface and the top of the ridge). L_{i} is the length of ice floes and L_{w} is the distance between ice floes. $\kappa = 0.4$ denotes the von Karman constant and ρ is the air density. $z_{0\mathrm{w}}$ and $z_{0\mathrm{i}}$ denote the roughness length of water and sea ice, respectively. $z_{0\mathrm{i}}$ is prescribed constant

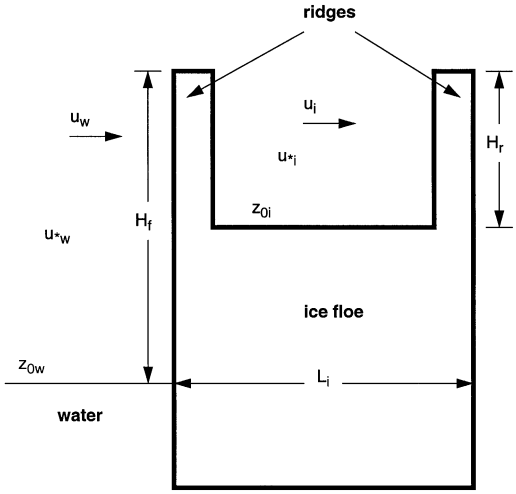

Fig. 1. Schematic representation of the new form drag parameterization.

($z_{0\mathrm{i}} = 10^{-3}$ m) whereas for water we use $z_{0\mathrm{w}} = \max(k_{\mathrm{c}} u_{*\mathrm{w}}^2/g,\ 1.5\times10^{-5}\ \mathrm{m})$ (Charnock, 1955; Clarke, 1970) with $k_{\mathrm{c}} = 0.018$ (Wu, 1980) and g the acceleration due to gravity. The friction velocities $u_{*\mathrm{w}}$ and $u_{*\mathrm{i}}$ determine the skin drag of water and ice, respectively. They are calculated within the flux averaging procedure explained in the next section. $\psi_{\mathrm{m,w}}$ and $\psi_{\mathrm{m,i}}$ are the stability functions of momentum over open water and over sea ice, respectively.

The form drag [eq. (1)] depends on the coefficient of resistance c_{w}. H-BG 88 use $c_{\mathrm{w}} = 1$. Observations of Banke and Smith (1975) and of Garbrecht et al. (1999), however, indicate that this value is much too large for small ice ridges. For this reason we use the value $c_{\mathrm{w}} = 0.37$ derived by Garbrecht (personal communication) from aircraft observed turbulent fluxes over the MIZ (Hartmann et al., 1994). This value also agrees reasonably well with the observations of Banke and Smith (1975) for small ridges.

3.2. *Turbulent fluxes over ice–water surfaces: the concept of flux averaging*

Mean surface fluxes over inhomogeneous surfaces are determined in METRAS with the so-called flux averaging method as the function of blending height l_{b}. The blending height is defined as the lowest level at which due to mixing

processes a nearly horizontally homogeneous flow exists over the inhomogeneous surface. Our flux averaging scheme including the calculation of l_b basically follows Claussen (1990, 1991a, 1991b) and von Salzen et al. (1996). However, in the present study, we additionally account for the momentum flux due to form drag in the calculation of l_b.

The mean turbulent surface flux of momentum F_m is given by

$$F_m = -A_w \rho u_{*w}^2 - A_i \rho u_{*i}^2 - F_d, \tag{2}$$

where A_w and A_i denote the concentration of water and ice, respectively ($A_w + A_i = 1$). Following Claussen's (1990, 1991a, 1991b) concept we assume a mean logarithmic profile $u(z)$ which is defined by the effective roughness length z_{0e} and the effective friction velocity u_{*e}. The values of z_{0e} and u_{*e} can be derived with the additional assumption of logarithmic wind profiles over water and ice. It is supposed that

$$u(l_b) = u_w(l_b) = u_i(l_b), \tag{3}$$

where u_w(z) and u_i(z) are the logarithmic wind profiles below the blending height over water and ice which are characterized by the local roughness lengths z_{0w} and z_{0i} and by the local friction velocities u_{*w} and u_{*i}. The individual fluxes can be determined with this assumption as

$$F_{m,j} = -\rho u_{*j}^2 = -\rho \kappa^2 u(l_b)^2 \frac{1}{[\ln(l_b/z_{0j}) - \psi_{m,j}]^2}, \tag{4}$$

where j refers to either water ($j = w$) or ice ($j = i$). The wind velocity at the blending height is obtained from

$$\frac{u(l_b)}{u(z_p)} = \frac{\ln(l_b/z_{0e})}{\ln(z_p/z_{0e})}. \tag{5}$$

Herein $u(z_p)$ is the mean wind velocity at the first model grid point above the surface. Inserting eq. (5) into eq. (4) results in

$$u_{*j} = \frac{\kappa\, u(z_p) \ln(l_b/z_{0e})}{\ln(z_p/z_{0e})[\ln(l_b/z_{0j}) - \psi_{m,j}]}. \tag{6}$$

Thus, the individual friction velocities can be calculated if l_b and z_{0e} are known. These parameters can be determined as described in the following.

If, as in Claussen (1990, 1991a, 1991b), the effect of stratification on l_b and z_{0e} is neglected, the flux over the ice–water surface is given by

$$\begin{aligned} F_m &= -\rho\kappa^2 u(l_b)^2 \left(A_w \frac{1}{[\ln(l_b/z_{0w})]^2} + A_i \frac{1}{[\ln(l_b/z_{0i})]^2} \right) - F_{d,n} \\ &= -\rho\kappa^2 u(l_b)^2 \frac{1}{[\ln(l_b/z_{0e})]^2} \end{aligned} \tag{7}$$

which follows from eqs. (2) and (4) with $\psi_{m,j} = 0$ if the three logarithmic wind profiles introduced above are used. $F_{d,n}$ denotes the form drag for neutral stratification only which is calculated from eq. (1) by solving the integrals analytically. Consequently, eq. (7) can be rewritten as

$$\begin{aligned} \frac{1}{\left(\ln \frac{l_b}{z_{0e}}\right)^2} = {} & \frac{1}{\left(\ln \frac{l_b}{z_{0w}}\right)^2} \left[A_w + \frac{c_w H_f}{\kappa^2 (L_i + L_w)} \right. \\ & \times \left(1 - \exp\left(-0.18 \frac{L_w}{H_f} \right) \right)^2 \\ & \left. \times \left(\left(\ln \frac{H_f}{z_{0w}} - 1 \right)^2 + 1 - 2 \frac{z_{0w}}{H_f} \right) \right] \\ & + \frac{1}{\left(\ln \frac{l_b}{z_{0i}}\right)^2} \left[A_i + \frac{c_w H_r}{\kappa^2 (L_i + L_w)} \right. \\ & \times \left(1 - \exp\left(-0.18 \frac{L_i}{H_r} \right) \right)^2 \\ & \left. \times \left(\left(\ln \frac{H_r}{z_{0i}} - 1 \right)^2 + 1 - 2 \frac{z_{0i}}{H_r} \right) \right]. \end{aligned} \tag{8}$$

A second equation with the unknown parameters l_b and z_{0e} was derived by Claussen (1991b) on the basis of results obtained with a microscale flow model. It was shown that the equation

$$\frac{l_b}{L_c} \left(\ln \frac{l_b}{z_{0e}} \right) = \kappa c_b \quad \text{with} \quad c_b = 1.75 \tag{9}$$

is approximately valid for the blending height. Herein L_c is the horizontal scale of roughness variations which we set to 300 m in the MIZ. The blending height and the effective roughness length can be calculated now by an iterative solution of eqs. (8) and (9).

3.3. *Parameterization of momentum flux in sea ice models*

Equation (1) is based on the assumption that the form drag has the same value per unit area over ice and over water within one model grid cell. For the mean atmospheric flux within one grid cell it makes no difference if we assume that the whole form drag modifies the flux over ice (or water) alone. However, if we consider the momentum balance equation of a dynamic sea ice model (Hibler, 1979), the whole form drag due to floe edges and ridges has to be related only to the area of ice floes because the form drag causes a transformation of momentum from the atmospheric motion into the ice drift. Thus, the surface wind stress in sea ice models reads

$$\tau_i = \rho u_{*i}^2 + \frac{1}{A_i} F_d \,. \tag{10}$$

This equation gives the link between the new parameterization of surface drag and its application in sea ice models.

The form drag F_d follows from eq. (1) and u_{*i} from eqs. (8), (9) and (6). Equations (1) and (6) require the knowledge of wind, temperature and humidity in the atmospheric surface layer. For sea ice models, these forcing variables are usually taken from atmospheric models or from (re-)analysis data. The freeboard height can be derived from the ice thickness calculated by sea ice models. A major problem might be the determination of the flow length and the distance between ice floes. These variables are not routinely provided by most sea ice models and have thus to be prescribed.

4. Observed data and model setup

The model METRAS is applied with and without the new surface drag parameterization to the flow over the MIZ in the Fram Strait region near Svalbard. Aircraft observations during meteorological conditions of cold-air outbreaks are available for this region from the two campaigns REFLEX I, II (Radiation and Eddy Flux Experiment, Hartmann et al., 1992; Kottmeier et al., 1994) for the validation of the new parameterization.

Mean drag coefficients c_d have been determined from all flights (see next section) as function of the sea ice concentration (Fig. 2). Each of the observed mean c_d-values in Fig. 2 results from several hundred km flight distance near the surface. Since the c_d-data comprise the results of flights carried out on different days, the model is run with meteorological and sea ice conditions which were typical for the whole measuring period rather than for one specific day.

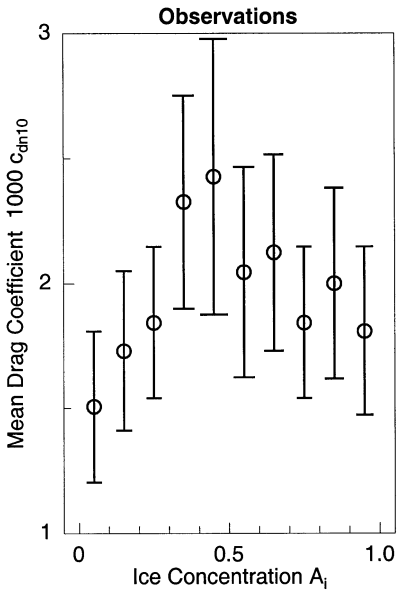

Fig. 2. Mean neutral drag coefficients at 10 m height c_{dn10} derived from observations (Hartmann et al., 1994; Kottmeier et al., 1994) as a function of ice concentration A_i.

4.1. *Meteorological conditions*

Profiles of wind, temperature and humidity, measured about 20 km upstream of the MIZ over regions with nearly 100% ice concentration, are available for some days of the campaigns. They show typically a shallow boundary layer of about 100–300 m height capped by a strong inversion. The observed profiles are used in the 1D version of METRAS to calculate inflow profiles at the northern boundary of the 2D model. The sea ice surface temperature derived from the observations is prescribed to be constant in the whole domain. Sea water is assumed to be at its freezing point of $T_w = -1.8\,^{\circ}\mathrm{C}$ because the model runs refer primarily to meteorological conditions occuring in winter. Four cases with different boundary condi-

tions and initial conditions are considered. In the first three cases, the geostrophic wind velocity is set to $10\,\mathrm{m\,s^{-1}}$ from north ($u_g = 0\,\mathrm{m\,s^{-1}}$, $v_g = -10\,\mathrm{m\,s^{-1}}$). Hence, the direction of the geostrophic wind is perpendicular to the east–west orientated ice edge.

In the first case (denoted as strong convective case hereafter), the sea ice surface temperature is $-34\,^{\circ}\mathrm{C}$, which leads to strong convection over the MIZ due to heating from the water surface. This situation was typical for the campaign REFLEX II (March/April 1993) from which most of the c_d-data result.

The second case (called convective case) refers to the conditions in October 1991 during REFLEX I. Here, the sea ice surface temperature was typically $-19\,^{\circ}\mathrm{C}$, which also leads to convection over the MIZ and over the open ocean.

In the third case (the neutral case), we use a value of $T_i = -1.8\,^{\circ}\mathrm{C}$. Hence, the near-surface stratification is neutral over both sea ice and water. The inflow profiles of heat and humidity also refer in this case to observed ones (summer campaign REFLEX III, Hartmann et al., 1997). However, during REFLEX III no drag measurements were carried out.

Case four differs from case one only with respect to the prescribed geostrophic wind. An angle of 45° is assumed between the geostrophic wind ($u_g = 5\,\mathrm{m\,s^{-1}}$, $v_g = -5\,\mathrm{m\,s^{-1}}$) and the orientation of the ice edge. This case is called case with oblique wind hereafter.

The prescribed geostrophic wind (case with perpendicular and case with oblique wind) is close to observations during REFLEX.

4.2. Sea ice conditions

For the present studies the model is used with a north-south orientated 2D domain of 280 km extension including the MIZ. To minimize the influence of the inflow and outflow boundaries an area with constant ice concentration is prescribed at the northern ($A_i = 100\%$) and the southern end ($A_i = 0\%$) of the domain. We consider two different MIZs, both 76 km long with A_i close to typically observed fields during REFLEX (Fig. 3). In our first case (MIZ1), A_i decreases linearly towards the open ocean. In a second case (MIZ2), A_i ranges from 0.95 to 0.80 within the first 56 km and then decreases within the next 20 km to zero (open ocean).

Freeboard heights and floe lengths are parameterized according to Mai (1995) on the basis of aircraft laser altimeter measurements and observations with a linescan camera during the REFLEX campaigns as:

$$\begin{aligned} H_f &= 0.49[1.0 - \exp(-5.9A_i)] \quad (H_f \text{ in m}) \\ H_r &= 0.5H_f \\ L_i &= 31H_f/(1 - A_i) \\ L_w &= L_i(1 - A_i)/A_i. \end{aligned} \tag{11}$$

Figure 4 shows the freeboard height H_f and the floe length L_i as function of the ice concentration A_i. Typically, in the MIZs observed during REFLEX L_i strongly increases with A_i, and the floe lengths vary between about 300 m for $A_i = 0.95$ (also used for $A_i = 1$) and 4 m for $A_i = 0.05$. H_f changes from 13 cm at $A_i = 0.05$ to $H_f = 49$ cm at $A_i = 0.95$.

5. Drag coefficients

Very often the surface momentum flux is calculated via the drag coefficient c_d with

$$F_m = -\rho c_d(z)u(z)^2 \quad \text{and} \quad c_d(z) = \frac{u_*^2}{u(z)^2}. \tag{12}$$

Although only eq. (12) is consistent with Monin–Obukhov theory, in sea ice/ocean models c_d is often prescribed constant.

Usually, the c_d-values are referred to $z = 10$ m. If we calculate u_* in eq. (12) with the flux averaging concept, a c_d-value including form drag can be derived as

$$c_{d10} = \frac{A_w u_{*w}^2 + A_i u_{*i}^2 + F_d/\rho}{(u_{10})^2}. \tag{13}$$

Herein u_{10} is the wind velocity at 10 m height (the first grid point above the surface in our model). Note that this definition of u_{10} is different from that used by Mai et al. (1996). They set u_{10} equal to the wind speed over water, which is only an approximation because, especially over larger floes, the wind can strongly differ from that over water.

Only the determination of c_d by means of eq. (13) is equivalent to the concept of form drag and flux averaging derived in Section 3. A flux

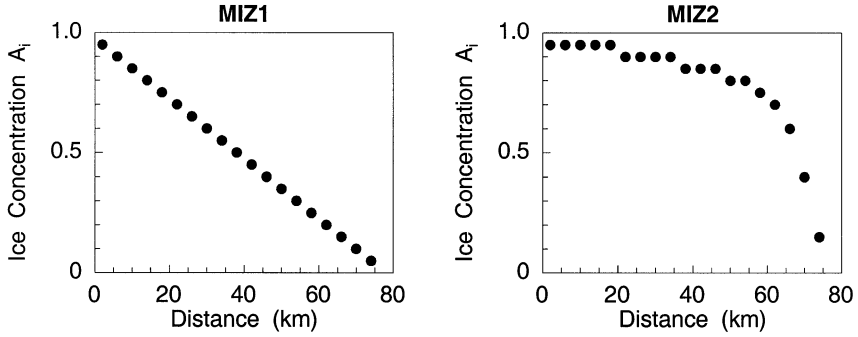

Fig. 3. Prescribed ice concentration A_i as a function of the distance from the northern edge of the marginal ice zones MIZ1 and MIZ2, respectively. Both curves are approximations of observed marginal ice zones near Svalbard (Mai, 1995).

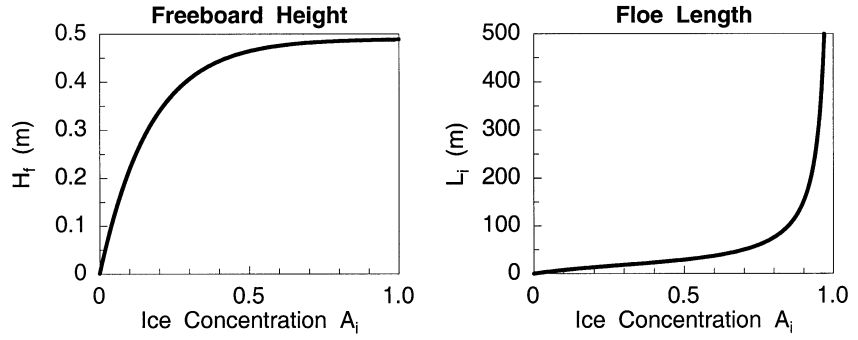

Fig. 4. Freeboard height H_f and floe length L_i as a function of ice concentration A_i calculated with eq. (11).

averaging method, however, cannot be used for the determination of c_d-values from observed fluxes over the MIZ. Observed c_d-values have to be calculated from

$$c_{d10} = \frac{\langle u_*^2 \rangle}{\langle u_{10} \rangle^2}, \tag{14}$$

where $\langle\ \rangle$ denotes an average over a flight leg (with 10 km length for the REFLEX cases) for which homogeneous turbulence is assumed. The average u_*^2 is calculated from the observed covariances $\overline{u'w'}$ and $\overline{v'w'}$ which refer to the horizontal wind averaged over the total flight leg. Thus, $\langle u_*^2 \rangle$ is different from the concentration weighted mean value which results from the flux averaging method. For an application of this method to observed data a separate determination of fluxes over ice and over water within a 10 km flight leg would be necessary. This is not possible for statistical reasons. At ice concentrations of 90% the flight length over open water would only amount to 1 km which is too short a distance for an accurate flux determination.

In literature, c_d-values are usually referred to neutral stratification and to 10 m height. Over homogeneous terrain the neutral values can be derived from observed fluxes by introducing stability corrected logarithmic wind profiles which leads to

$$c_{dn10} = \kappa^2 \left[\frac{\kappa \langle u_{10} \rangle}{\langle u_* \rangle} + \psi_m \left(\frac{10}{\langle L \rangle} \right) \right]^{-2}, \tag{15}$$

where L is the Monin–Obukhov length. This method was also used to transform the observed c_d-values from REFLEX to the neutral ones shown in Fig. 2. It can be simply shown, however, that drag coefficients calculated with eq. (15) are not completely independent of stratification if the surface characteristics like temperature and roughness vary strongly on the flight leg. Since for neutral stratification on average ψ_m would be zero in eq. (15), no stability correction would be carried

out. However, in such a case, a flight leg can consist of stable and unstable segments, with fluxes being significantly different from fluxes at neutral conditions in each segment. Hence, $\langle u_* \rangle$ and thus c_{dn10} would be significantly different from values valid for neutral stratification in each segment.

A comparison of modelled and observed neutral drag coefficients is carried out for this reason as follows. We first use METRAS to calculate the flow field with our new surface drag parameterization and the flux averaging method. When the model results are quasi-stationary we calculate c_{dn10}-values diagnostically with eq. (15). Here the averages $\langle\ \rangle$ correspond to grid cell averages. Consequently, the c_{dn10}-values diagnosed from the model results also refer to a stratification which is neutral only on average.

6. Model results

Most of the results which we discuss in the following have been obtained with the broader marginal ice zone MIZ1. MIZ2 is only used to show that the drag coefficients are not very sensitive to deviations from MIZ1 which is regarded here as typical.

6.1. *The boundary layer over the MIZ and influence of form drag*

Figures 5 and 6 show vertical cross-sections of the modelled potential temperature and of the absolute value of the horizontal wind velocity, respectively, for the strong convective cases, where the geostrophic wind is perpendicular (upper

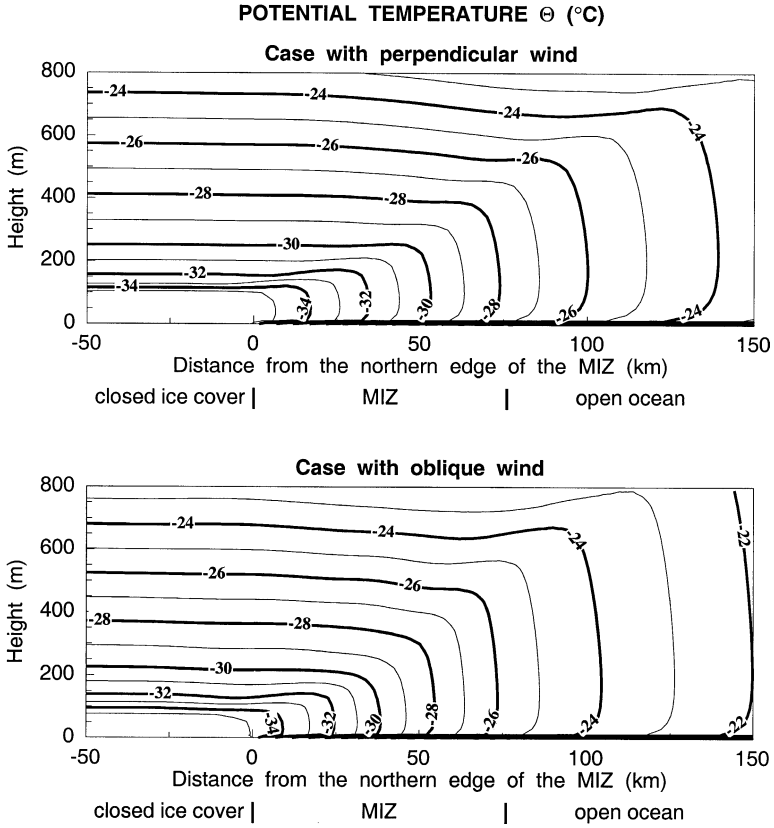

Fig. 5. Potential temperature Θ as a function of height and distance from the northern edge of MIZ1 for $T_i = -34\,^{\circ}\mathrm{C}$ (strong convective case) calculated with the new parameterization of form drag. The geostrophic wind is perpendicular ($u_g = 0\ \mathrm{m\,s^{-1}}$, $v_g = -10\ \mathrm{m\,s^{-1}}$) to the ice edge (upper panel) and oblique ($u_g = 5\ \mathrm{m\,s^{-1}}$, $v_g = -5\ \mathrm{m\,s^{-1}}$) to the ice edge (lower panel).

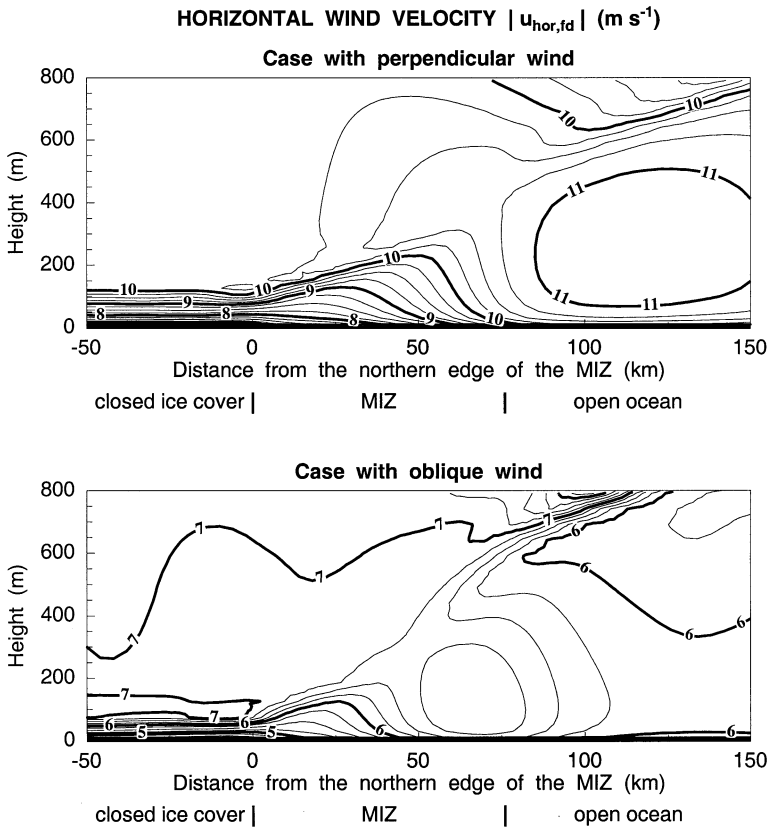

Fig. 6. Horizontal wind velocity $|\boldsymbol{u}_{\mathrm{hor,fd}}|$ as a function of height and distance from the northern edge of MIZ1 for $T_{\mathrm{i}} = -34\,^{\circ}\mathrm{C}$ (strong convective case) calculated with the new parameterization of form drag. The geostrophic wind is perpendicular ($u_{\mathrm{g}} = 0\ \mathrm{m\,s^{-1}}$, $v_{\mathrm{g}} = -10\ \mathrm{m\,s^{-1}}$) to the ice edge (upper panel) and oblique ($u_{\mathrm{g}} = 5\ \mathrm{m\,s^{-1}}$, $v_{\mathrm{g}} = -5\ \mathrm{m\,s^{-1}}$) to the ice edge (lower panel).

panel) and oblique (lower panel) to the ice edge. In both cases the new surface drag parameterization is applied. A typical convective boundary layer with increasing mixed layer height towards the south (right end of the figures) develops over the MIZ and over open water. An inclusion of form drag does not alter the well known structure of the temperature and wind field in the convective boundary layer. In accordance with earlier findings a maximum value of wind velocity still occurs south of the region with closed pack ice. Figure 7 shows a vertical cross-section of the modelled fluxes of sensible heat for the case with geostrophic wind perpendicular to the ice edge. Due to the strong temperature difference between the atmosphere and the water large fluxes occur with a maximum value of about 500 W m^{-2} at the southern end of the MIZ. The increase of near-surface fluxes over the MIZ is caused by the decrease of ice concentration.

Similar results of the general boundary layer development obtained with the model METRAS for the conditions of cold-air outbreaks have already been discussed by Lüpkes and Schlünzen (1996), who, however, neglected the form drag. They showed that the temperature evolution in the convective boundary layer south of the pack ice agreed well with observed data. This was possible by an inclusion of countergradient heat fluxes in their nonlocal parameterization of turbulent fluxes above the surface layer which is also used in the present study. Countergradient heat

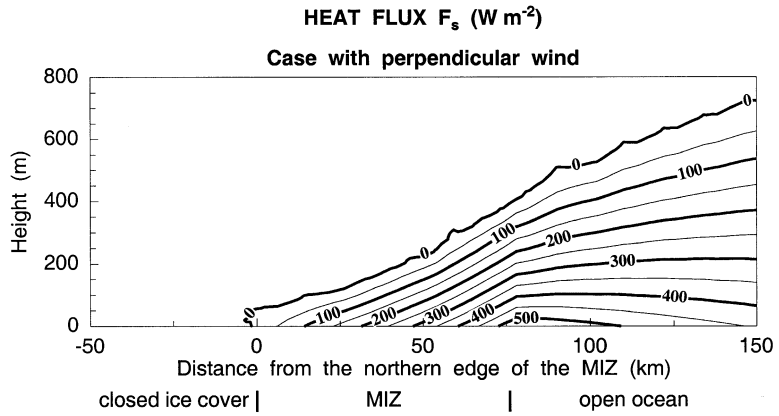

Fig. 7. Turbulent flux of sensible heat F_s as a function of height and distance from the northern edge of MIZ1 for $T_i = -34\,^{\circ}\mathrm{C}$ (strong convective case) calculated with the new parameterization of form drag. The geostrophic wind is perpendicular ($u_g = 0\ \mathrm{m\,s^{-1}}$, $v_g = -10\ \mathrm{m\,s^{-1}}$) to the ice edge.

fluxes can cause a slight increase of potential temperature with height in the mixed layer as visible in Fig. 5.

Model runs were carried out with and without the form drag parameterization. In both cases the flux averaging method was applied. The temperature field is only slightly changed by form drag effects. Differences with respect to temperature (not shown here) are not larger than 0.2 K. This is due to the small impact of the form drag on the heat fluxes (Fig. 8). There are, however, more significant differences between the modelled absolute values of the wind velocity obtained with and without form drag (Fig. 9). While looking at Fig. 9 it should be kept in mind that our parameterization is developed for the MIZ only. An additional inclusion of the form drag of ridges in the pack ice region with, e.g., the concept of Garbrecht et al. (1999) would also alter the results north of the MIZ.

Obviously, the form drag influence on the wind velocities is much larger in case of geostrophic wind oblique to the ice edge (Fig. 9), because the flow in the boundary layer has more time to adjust to the lower boundary conditions. Within the MIZ the differences amount to up to $1.1\ \mathrm{m\,s^{-1}}$ (16% of geostrophic wind) near the surface in the case with geostrophic wind oblique to the ice edge, but they amount to only up to $0.5\ \mathrm{m\,s^{-1}}$ (5% of geostrophic wind) if the geostrophic wind is perpendicular to the ice edge. In both cases the differences between the results obtained with and

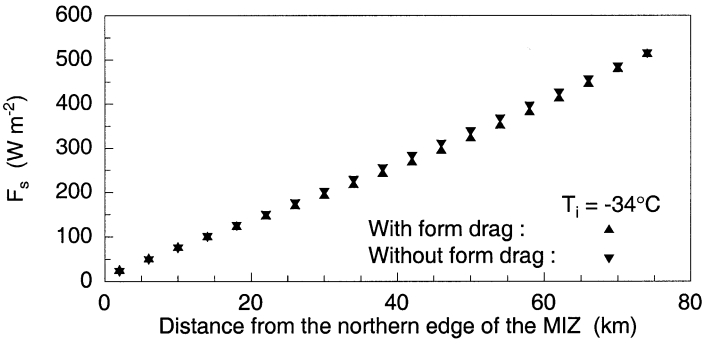

Fig. 8. Turbulent surface flux of sensible heat F_s as a function of the distance from the northern edge of MIZ1. The simulations are carried out with and without the new parameterization of form drag for $T_i = -34\,^{\circ}\mathrm{C}$ (strong convective case). The geostrophic wind is perpendicular to the ice edge.

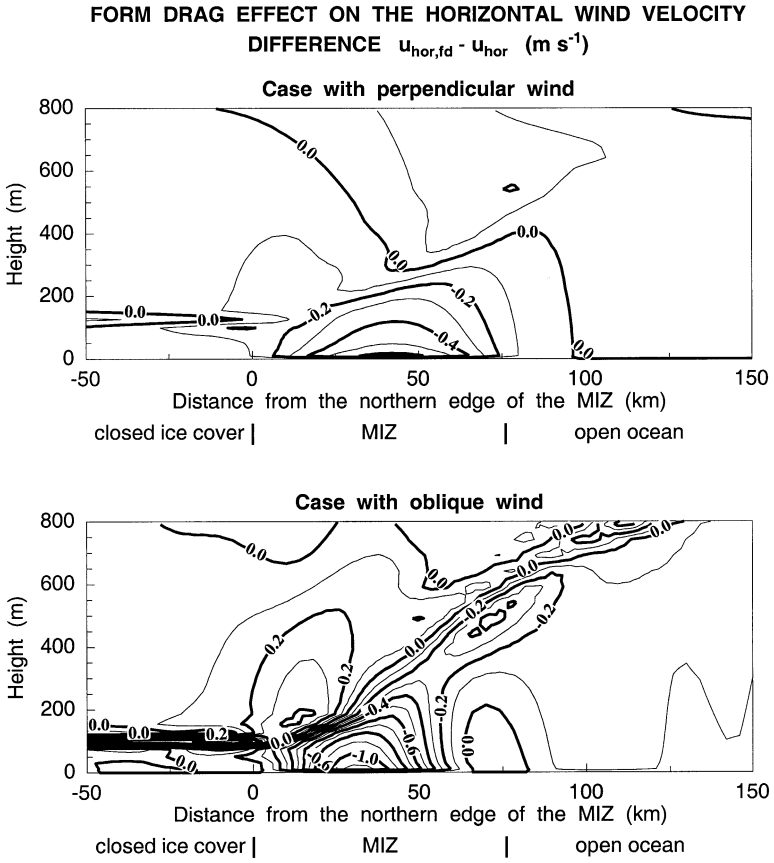

Fig. 9. Difference of horizontal wind velocity between a simulation with form drag ($u_{\mathrm{hor,fd}}$) and without form drag (u_{hor}) as a function of height and distance from the northern edge of MIZ1 for $T_{\mathrm{i}} = -34\,^{\circ}\mathrm{C}$ (strong convective case). The geostrophic wind is perpendicular ($u_{\mathrm{g}} = 0\ \mathrm{m\,s^{-1}}$, $v_{\mathrm{g}} = -10\ \mathrm{m\,s^{-1}}$) to the ice edge (upper panel) and oblique ($u_{\mathrm{g}} = 5\ \mathrm{m\,s^{-1}}$, $v_{\mathrm{g}} = -5\ \mathrm{m\,s^{-1}}$) to the ice edge (lower panel).

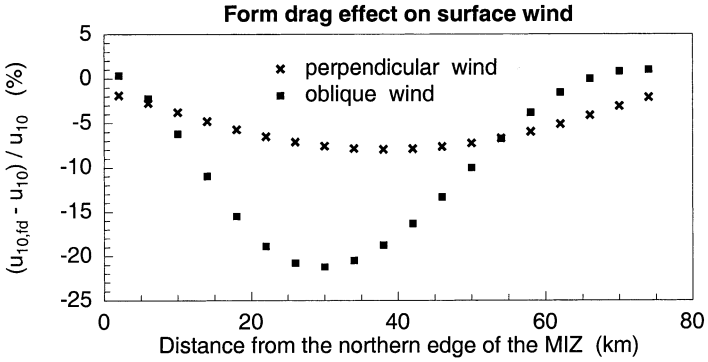

Fig. 10. Relative difference of the horizontal wind velocity at 10 m height between a simulation with form drag ($u_{10,\mathrm{fd}}$) and without form drag (u_{10}) as a function of distance from the northern edge of MIZ1 for $T_{\mathrm{i}} = -34\,^{\circ}\mathrm{C}$ (strong convective case). The geostrophic wind is perpendicular to the ice edge (crosses) and oblique to the ice edge (squares).

without form drag are visible in the whole boundary layer over the MIZ. However, the differences in the wind velocity are most pronounced near the surface. The relative difference of the wind at 10 m height between the model runs with and without form drag can reach 20% in case of oblique geostrophic wind (Fig. 10). Hence, an inclusion of a form drag parameterization in coupled atmosphere–ice models would probably influence the ice drift considerably.

Figure 11 demonstrates the effect of stratification and of form drag on the surface momentum fluxes for the cases with geostrophic wind perpendicular to the ice edge. In both runs with and without form drag the fluxes remain approximately constant with increasing distance from the northern end of the MIZ in the neutral case. In the strong convective cases, however, the fluxes increase towards the open ocean. This is caused by the acceleration of the flow over open water which does not exist for neutral stratification. Independent of stratification, there is a larger mean momentum flux at the ice–water surface if form drag is included in the model. The maximum difference between the fluxes of the model runs with and without form drag amounts to about 25% of the modelled skin drag. It occurs at ice concentrations of about 45% to 55% (at about 40 km distance in Fig. 11) depending on thermal stratification. This differs from a study of H-BG 88, due to which a maximum form drag occurs at 73% ice concentration for floes observed in the Fram Strait in July 1983. However, this difference can be easily explained by differences in the ice morphology (floe length, freeboard height).

The maximum influence of form drag on sea ice wind stress occurs in the case with strong unstable stratification and with wind oblique to the ice edge (Fig. 12). Under such conditions the wind stress on sea ice is modified by at least 100% for ice concentrations less than 50% (at about 40 km distance in Fig. 12) if form drag is taken into account. In all cases which we investigated the influence of form drag depends on the sea ice concentration, and it is largest at about 65 km south of the northern edge of the MIZ where the sea ice concentration is 15–20%. The results for the sea ice wind stress indicate again that the consideration of form drag is not only important for atmospheric models but also for sea ice models. Neglecting the form drag, the atmospheric forcing of the ice motion is strongly underestimated, especially for ice concentrations below 30%. Furthermore, the horizontal divergence of the wind stress on sea ice is only significantly different from zero if the form drag is taken into account. Such a non-zero flux divergence could have an effect on the widening of the MIZ during off-ice wind.

6.2. *Influence of form drag on drag coefficients*

Figure 13 shows mean drag coefficients c_{dn10} calculated with eq. (15) from observations and from model results as function of A_i. The simulations are carried out with form drag (right panel)

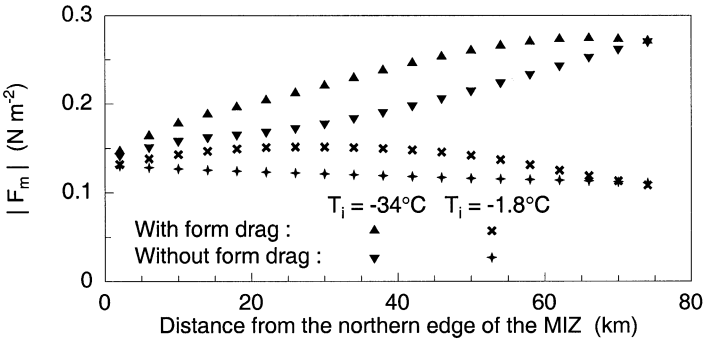

Fig. 11. Absolute value of the turbulent surface momentum flux $|F_m|$ as a function of the distance from the northern edge of MIZ1. The simulations are carried out with and without the new parameterization of form drag for both $T_i = -34\,^{\circ}C$ (strong convective case) and $T_i = -1.8\,^{\circ}C$ (neutral case). The geostrophic wind is perpendicular to the ice edge.

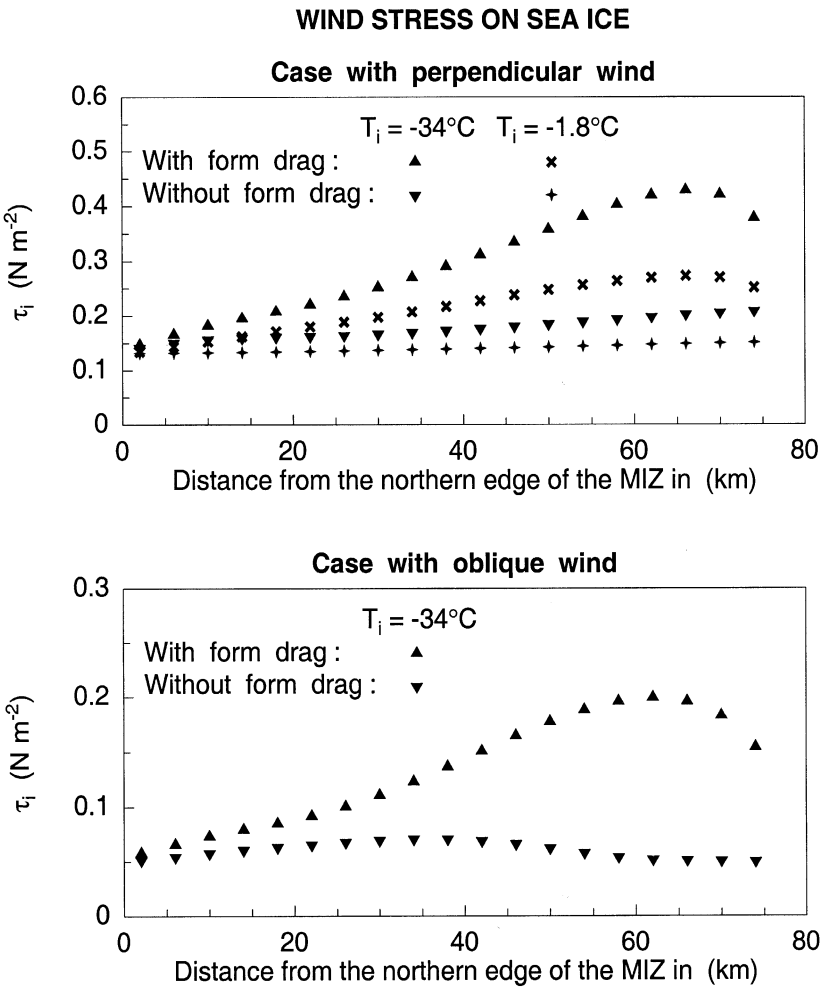

Fig. 12. Wind stress on sea ice τ_i as a function of the distance from the northern edge of MIZ1. The simulations are carried out with and without the new parameterization of form drag. In the upper panel, the geostrophic wind is perpendicular ($u_g = 0\ \mathrm{m\ s^{-1}}$, $v_g = -10\ \mathrm{m\ s^{-1}}$) to the ice edge and the sea ice surface temperature is $T_i = -34\ ^\circ\mathrm{C}$ (strong convective case) and $T_i = -1.8\ ^\circ\mathrm{C}$ (neutral case). In the lower panel, the geostrophic wind is oblique ($u_g = 5\ \mathrm{m\ s^{-1}}$, $v_g = -5\ \mathrm{m\ s^{-1}}$) to the ice edge and the sea ice surface temperature is $T_i = -34\ ^\circ\mathrm{C}$ (strong convective case).

and without form drag (left panel) for the three cases (see Section 4) with perpendicular geostrophic wind to the ice edge and with different sea ice surface temperatures (strong convective, convective and neutral case). The influence of the geostrophic wind direction on the drag coefficients is negligibly small. For this reason, only results for geostrophic wind perpendicular to the ice edge are discussed. Obviously, the modelled c_{dn10}-values depend on stratification and hence on the sea ice surface temperature. As explained in Section 5, this effect results from the application of eq. (15). The values for the case with neutral stratification over ice and over water (uppermost curve in the right panel of Fig. 13) are significantly larger than those obtained with eq. (15) for the convective cases. Since most of the observed c_{dn10}-values were derived from strong convective cases, the most meaningful comparison is between our model results for the strong convective case and the observed data. Obviously, a neglection of form drag leads to an underestimation of the mean drag

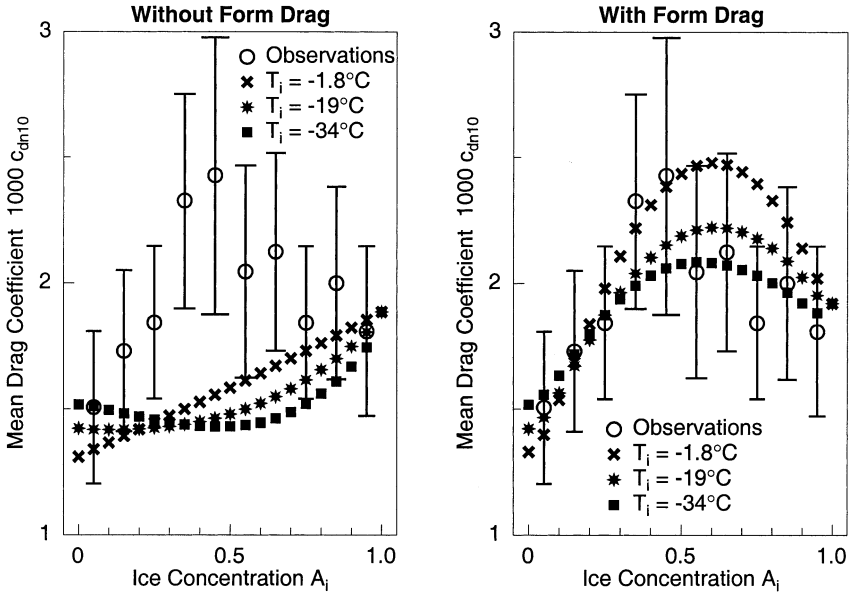

Fig. 13. Mean drag coefficients at 10 m height c_{dn10} calculated with eq. (15) from observations and from model results as a function of ice concentration A_i. The simulations are carried out with (right panel) and without (left panel) the new parameterization of form drag for MIZ1 and for three different sea ice surface temperatures.

coefficients in the MIZ (left panel of Fig. 13), and the inclusion of the form drag can approximately explain the observed dependence of c_{dn10} on ice concentration. The observed maximum of c_{dn10} occurs at ice concentrations of about 45% whereas the modelled maximum value is between 55% and 60%. This difference is within the observational error (see Fig. 13). For larger ice concentrations the drag coefficients decrease with A_i for two reasons. The first one is the sheltering effect of ice floes with small distances from each other. The second one is the increase of the floe diameter with increasing ice concentration due to eq. (11), which is equivalent to a decrease of floe edges per unit area.

The results in Fig. 13 indicate that aircraft-observed c_d-values over the MIZ which are reduced to neutral values underestimate the real c_{dn10} by up to 20% in the case of strong differences between the surface temperatures of ice and ocean. In general, the strength of this effect depends on the ice concentration and on the stratification.

The sensitivity of the modelled mean drag coefficients to the coefficients of resistance c_w in the form drag parameterization is demonstrated in Fig. 14. The squares refer to the new para-

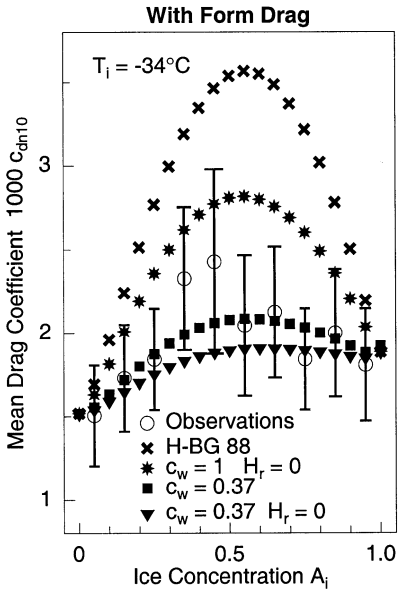

Fig. 14. Mean drag coefficients at 10 m height c_{dn10} calculated with eq. (15) from observations and from model results for different coefficients of resistance c_w in the form drag parameterization as a function of ice concentration A_i. The simulations are carried out for MIZ1 and $T_i = -34\,^{\circ}\mathrm{C}$ (strong convective case).

meterization proposed in Section 3. Obviously, with this choice of c_w the modelled curve and observed data agree best. Larger differences occur only at sea ice concentrations of about $A_i = 40\%$. For the lowest curve we used the new parameterization but set $H_r = 0$ which means that the ridge at the leeward side of the floe is neglected. The difference between both curves is not larger than 10% but the full new parameterization with $H_r \neq 0$ seems to agree slightly better with the observations. Additionally, Fig. 14 contains two results (upper curves) for $c_w = 1$ and $H_r = 0$. These are the values used by H-BG 88. In contrast to the curve marked with stars the uppermost curve (crosses) additionally neglects the stratification in the form drag calculation [$\psi_m = 0$ in eq. (1)], and thus refers to the original H-BG 88 drag parameterization. Obviously, the latter strongly overestimates the mean drag coefficients.

It could be speculated whether the results obtained for the two marginal ice zones MIZ1 and MIZ2 results in different drag coefficients, because the skin drag roughness length over water is calculated with the Charnock formula. Hence, z_{0w} depends on the skin drag friction velocity, and for this reason also on the near surface wind velocity which is slightly different in the two cases. As Fig. 15 shows for the convective cases, there is, however, only a very small difference between the results obtained with MIZ1 and MIZ2.

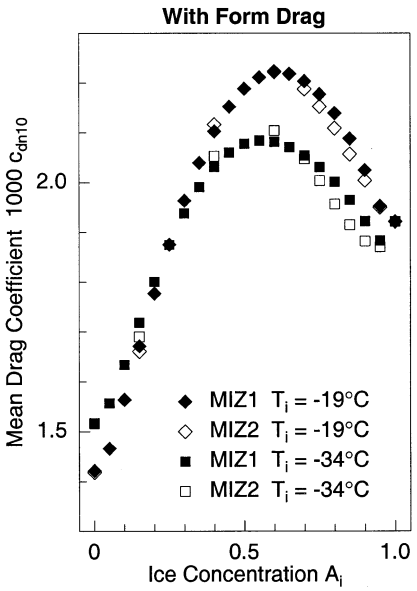

Fig. 15. Mean drag coefficients at 10 m height c_{dn10} calculated with eq. (15) from model results for the two different marginal ice zones MIZ1 and MIZ2 as a function of ice concentration A_i. The simulations are carried out with the new parameterization of form drag for $T_i = -34\,^\circ\mathrm{C}$ (strong convective case) and $T_i = -19\,^\circ\mathrm{C}$ (convective case), respectively.

7. Summary and conclusions

A new parameterization of surface drag over the MIZ has been derived which accounts for the form drag of floe edges. It combines the form drag parameterization of H-BG 88 with the so-called flux averaging method of Claussen (1990, 1991a, 1991b) for the determination of mean surface fluxes over inhomogeneous terrain. The individual subgridscale fluxes over ice and water are calculated as a function of the blending height, which is influenced by form drag. In the new parameterization three assumptions of the original concept of H-BG 88 are revised. First, we assume floes with pressure ridges at the edges instead of flat floes. Second, the coefficient of resistance of ice floes used in our parameterization is much smaller than that of H-BG 88. The third difference concerns the influence of thermal stratification on the form drag, which is accounted for in the new concept only. It turns out by comparison of modelled and observed mean drag coefficients that the second and third revisions have the largest effects on the drag coefficients. The assumption of a pressure ridge at the leeward floe edge also effects the results, but its influence is much smaller than those of the other assumptions.

Mean drag coefficients obtained from a model application to the MIZ with the new parameterization agree well with observations. A neglection of form drag leads to a strong underestimation of c_d-values. Use of the original concept of H-BG 88 results in an overestimation of the mean drag coefficients.

The model studies indicate that a method often used for transforming observed nonneutral drag coefficients into neutral ones does not work well over surfaces with strong temperature inhomogeneity. The differences between the transformed drag coefficients and those for neutral stratification over ice and over water are largest when the transformed coefficients result from drag coeffi-

cients observed originally during strong convective stratification. Thus, it could be useful to carry out additional aircraft observations during neutral conditions over water and ice which are typically met in the Arctic summer.

Drag coefficients as a function of the sea ice concentration could be of interest for models in which the surface fluxes are determined from mean surface parameters rather than from a flux averaging method. In such models, neutral c_d-values should be used which result from our model run for the neutral case considered in the previous section (uppermost curve in Fig. 13). With respect to a parameterization of c_d-values as a function of the ice concentration, the results shown in Fig. 15 are encouraging because the influence of the specific ice distribution on the drag coefficients seems to be small, at least in the MIZ. However, it should be stressed that there is a strong dependence of momentum fluxes and hence of drag coefficients on the floe length and on the freeboard height which we did not discuss in the present paper. It should be also kept in mind that an application of mean c_d-values cannot reproduce heat fluxes directed upward when the stratification is neutral or stable on average within one grid cell. This is only possible with a flux averaging procedure.

The form drag can have a strong influence on the wind field over the MIZ and particularly on the sea ice wind stress. Hence, it could be worth incorporating the form drag of floe edges into coupled atmosphere–ice models to investigate its effect on the sea ice drift.

8. Acknowledgements

We thank Jörg Hartmann for providing us with the aircraft data. Valuable comments of an anonymous reviewer are gratefully acknowledged. This study was funded by the EU-project ARTIST (grant no. ENV4-CT97-0487).

REFERENCES

Arya, S. P. S. 1975. A drag-partition theory for determining the large-scale roughness parameter and wind stress on Arctic pack ice. *J. Geophys. Res.* **80**, 3447–3454.

Banke, E. G. and Smith, S. D. 1975. Measurement of form drag on ice ridges. *AIDJEX Bull.* **28**, 21–27.

Charnock, H. 1955. Wind stress on a water surface. *Q. J. R. Meteorol. Soc.* **81**, 639–640.

Clarke, R. H. 1970. Recommended methods for the treatment of the boundary layer in numerical models. *Aust. Meteor. Mag.* **18**, 51–71.

Claussen, M. 1990. Area-averaging of surface fluxes in a neutrally stratified, horizontally inhomogeneous atmospheric boundary layer. *Atm. Environ.* **24A**, 1349–1360.

Claussen, M. 1991a. Local advection processes in the surface layer of the marginal ice zone. *Boundary-Layer Meteorol.* **54**, 1–27.

Claussen, M. 1991b. Estimation of areally-averaged surface fluxes. *Boundary-Layer Meteorol.* **54**, 387–410.

Dyer, A. J. 1974. A review of flux–profile relationship. *Boundary-Layer Meteorol.* **7**, 363–372.

Dierking, W. 1995. Laser profiling of the ice surface topography during the winter Weddell Gyre study 1992. *J. Geophys. Res.* **100**, 4807–4820.

Garbrecht, T., Lüpkes, C., Augstein, E. and Wamser, C. 1999. The influence of a sea ice ridge on the low level air flow. *J. Geophys. Res.* **104 (D20)**, 24499–24507.

Hanssen-Bauer, I. and Gjessing, Y. T. 1988. Observations and model calculations of aerodynamic drag on sea ice in the Fram Strait. *Tellus* **40A**, 151–161.

Hartmann, J., Kottmeier, C. and Wamser, C. 1992. Radiation and eddy flux experiment 1991 (REFLEX I). *Reports on Polar Res.* Vol. 105, Alfred Wegener Institute, Bremerhaven, 72 pp.

Hartmann, J., Kottmeier, C., Wamser, C. and Augstein, E. 1994. Aircraft measured atmospheric momentum, heat and radiation fluxes over Arctic sea ice. In: *The polar oceans and their role in shaping the global environment* (eds O. M. Johannessen, R. D. Muench and J. E. Overland). American Geophysical Union, Washington, DC, 443–454.

Hartmann, J., Bochert, A., Freese, D., Kottmeier, C., Nagel, D. and Reuter, A. 1997. Radiation and eddy flux experiment 1995 (REFLEX III). *Reports on Polar Res.* Vol. 218, Alfred Wegener Institute, Bremerhaven, 74 pp.

Herbert, F. and Kramm, G. 1985. Trockene Deposition reaktionsträger Substanzen, beschrieben mit einem diagnostischen Modell der bodennahen Luftschicht. In: *Atmosphärische Spurenstoffe und ihr physikalisch-chemisches Verhalten* (eds. K. H. Becker and J. Löbel). Springer Press, Berlin, 264 pp.

Hibler, W. D., III 1979. A dynamic thermodynamic sea ice model. *J. Phys. Oceanogr.* **9**, 815–846.

Kottmeier, C., Hartmann, J., Wamser, C., Bochert, A., Lüpkes, C., Freese, D. and Cohrs, W. 1994. Radiation and eddy flux experiment 1993 (REFLEX II). *Reports on Polar Res.* Vol. 133, Alfred Wegener Institute, Bremerhaven, 62 pp.

Lüpkes, C. and Schlünzen, K. H. 1996. Modelling the

arctic convective boundary-layer with different turbulence parameterizations. *Boundary-Layer Meteorol.* **79**, 107–130.

Mai, S. 1995. Beziehungen zwischen geometrischer und aerodynamischer Oberflächenrauhigkeit arktischer Meereisflächen. *M.Sc. Thesis*, University of Bremen, 75 pp.

Mai, S., Wamser, C. and Kottmeier, C. 1996. Geometric and aerodynamic roughness of sea ice. *Boundary-Layer Meteorol.* **77**, 233–248.

Orlanski, I. 1976. A simple boundary condition for unbounded hyperbolic flows. *J. Compat. Phys.* **21**, 251–269.

Schlünzen, K. H. 1988. Das mesoskalige Transport- und Strömungsmodell 'METRAS' – Grundlagen, Validierung, Anwendung. *Geophysikalische Einzelschriften*, Vol. A88, Meteorological Institute, University of Hamburg, 139 pp.

Schlünzen, K. H. 1990. Numerical studies on the inland penetration of sea breeze fronts at a coastline with tidally flooded mudflats. *Beitr. Phys. Atmosph.* **63**, 243–256.

von Salzen, K., Claussen, M. and Schlünzen, K. H. 1996. Application of the concept of blending height to the calculation of surface fluxes in a mesoscale model. *Meteorol. Z.* **5**, 60–66.

Wefelmeier, C. 1992. Numerische Simulation mesoskaliger, dynamischer Wechselwirkungen zwischen Atmosphäre, Eis und Ozean. *Reports of the Institute for Meteorology and Climatology*, Vol. 42, University of Hannover, 141 pp.

Wu, J. 1980. Wind stress coefficients over sea surface near neutral conditions – a revisit. *J. Phys. Oceanogr.* **10**, 727–740.